VEHICLE SYSTEM DYNAMICS
https://doi.org/10.1080/00423114.2023.2264418

Validation of a novel bicycle simulator with realistic lateral and roll motion

Jelle Haasnoot[a,b], Riender Happee[a], Volkert van der Wijk[a] and Arend L. Schwab[a]

[a]Faculty of Mechanical Engineering, Delft University of Technology, Delft, Netherlands; [b]Tacx B.V., a Garmin Company, Oegstgeest, Netherlands

ABSTRACT

Bicycle simulators have been the subject of considerable research, however, few of these attempts have integrated direct balance control and realistic freedom of motion to deliver a real-world dynamic cycling experience. This study presents the BIKE (Bicycle Intrinsic Kinematics Emulator) system, a kinematic bicycle simulator, developed with the purpose of letting its users experience realistic steer, roll, yaw and sway motions. Motion is provided with Carvallo–Whipple bicycle model-based control of sway and yaw combined with passive steer and roll. This study validates the BIKE simulator by comparing cycling behaviour and subjective evaluation for the simulator with and without motion to outdoor tests with an instrumented bicycle. 15 participants of varying age and mass, performed straight-line cycling, at low (5 km/h) to high (40 km/h) velocities and zig-zag manoeuvres. Results show that users can successfully rely on existing cycling skills to use the simulator with motion. Objectively, in the kinematic sense, the simulator with motion performs similarly to an outdoor bicycle. Subjectively, the simulator performs better with motion and is experienced by riders as close to real outdoor cycling.

ARTICLE HISTORY
Received 29 March 2023
Revised 6 July 2023
Accepted 30 August 2023

KEYWORDS
Bicycle; simulation; dynamics; kinematics; modelling

1. Introduction

In recent years, indoor cycling simulators (or 'trainers', used as exercising equipment) have undergone great technical improvement. These devices, which allow their users to exercise cycling indoors, provide braking resistance to an eager athlete, similar to spinning bikes and ergometers in gyms. Manufacturers of these personal simulators strive for increasingly accurate representations of (both virtual and mechanical) bicycle motion, with some products already available on the market [1–3]. Tacx, a manufacturer of indoor cycling trainers, initiated this study, to develop a bicycle simulator incorporating more realistic physical motion, allowing for a more natural recreation of a cyclist's balancing behaviour and power delivery indoors.

Over the past decades, several bicycle simulators incorporating physical motion have been presented. Static frame setups with two controllable mechanical degrees of freedom on the bicycle prevail [4–11], where usually only the rear-wheel velocity and steering

CONTACT Arend L. Schwab a.l.schwab@tudelft.nl

angle are controllable by the user. Full-fledged Stewart platform-based simulators, with six or more degrees of freedom of the bicycle, have been developed as well, but are rarer [12–16].

The focus of these simulators appears to lie with the development of a realistic visual environment with bike motion based on rider steering control (usually the bicycle's steering angle, or force-based measurement of the applied steering torque). In most bicycle simulators, the roll angle of the bicycle is either fixed, only represented visually or a result from a modelled bicycle, and not directly controlled by cyclist body motion. Only the studies [8,13] report on the (lack of) degrees of freedom of their respective simulators. While both [8,13] claim to have developed realistic bicycle simulators, neither study provides subjective data to support those claims. A motorcycle simulator included effects of camera-based body lean on vehicle motion but found no significant effects on rider behaviour and perceived realism [17]. Other simulators allow some frame roll with passive stabilisation [9]. However, as far as we know, no study has attempted to design a bicycle simulator with physically accurate lateral bicycle kinematics where the rider is able to balance the bicycle directly through both steering and body motion.

The knowledge on how this balancing act works and how humans control bicycles has been around quite awhile. Schwab [18] provides a summary, paraphrased below. As early as 1820, it was found that to balance a bicycle, one had to steer into an undesired fall [19]. Laterally accelerating the support line of the bicycle is what primarily rights it, the acceleration generated by steering the front wheel of the bicycle [20]. Rankine [20] also found that to exert a lateral force with the bicycle in turning a corner (counteracting the centripetal force in performing a circular motion), riders must be able to lean the bicycle to compensate for this force, and afterwards compensate for this lean by steering. Upper-body lean contributes little to stabilisation, and the largest contributor to bicycle stability is considered to be the steering input. However, at very low speeds, knee-movements also aid in the stabilisation [21,22] and bike roll will affect the energy efficiency of pedalling.

Thus, the focus of our new simulator will lie on the integration and enactment of the degrees of freedom required for the lateral balance of a bicycle. That is being able to steer into the undesired fall (or roll motion), resulting in a yaw and lateral sway motion, hence accelerating the bicycle's support line and letting the cyclist laterally balance the bicycle. This study presents and validates a prototype bicycle simulator, where its user will be given the freedom to steer and balance the bicycle through steering and body interaction. We focus on steer, roll, yaw and sway motion. Sustained cornering, forward acceleration and braking are not part of the development focus in this study. We validate usability and realism with 15 participants comparing simulator and outdoor experiments and use a fixed indoor setup for reference.

Simulator design

This section describes the simulator design, starting with a definition of the simulator's requirements, followed by the physical realisation, the kinematic vehicle model, the motion control and the visualisation.

The novel simulator has to defer the path control and lateral balancing task of the bicycle to its user. The user then shall be able to control the bicycle similarly to when cycling on the open road. Concretely, the requirements for the simulator and vehicle model are:

(1) The simulator shall be designed with the degrees of freedom necessary to pedal and laterally balance the bicycle by steering and body interaction. This means that rear-frame roll, yaw, lateral motion and front-fork steer shall remain free to move in the simulator. Surge, heave and pitch motions are beyond the scope of this study.
(2) The simulator shall respond kinematically to a cyclist's control actions, through sensor-based input and state measurements. A motion response shall result from a vehicle model derived from a real bicycle's geometry and imposed boundary conditions.
(3) A braking unit shall provide an approximate resistance to the cyclist's pedalling, such that a proper simulation of forward acceleration and velocity can be provided to the user.
(4) A visualisation system shall, coupled with the braking unit resistance and rear-wheel velocity, give the user of the simulator a sense of forward velocity, and present the attained path and frame roll as a function of the steering and balance control actions of the rider.

The BIKE (Bicycle Intrinsic Kinematics Emulator) system was designed to meet these objectives with hardware and controls illustrated in Figures 1 and 3. The mechanical setup consists of a bicycle where the two contact points of the front and rear wheel are moved laterally by two active controlled linear motors. The two motors are controlled independently to generate yaw and lateral motion. Revolute joints at the contact points allow bicycle roll. An additional translational joint at the front contact point allows a small fore-aft motion of the front wheel contact point relative to the front lateral actuator.

The BIKE system functions as follows: the kinematic state of the bicycle, the steer angle δ, the rear frame roll angle θ and rear-wheel velocity v_R, are measured. This state is the input for the kinematic bicycle model which gives as output the desired lateral velocities of the rear and front wheel contact points. These velocities are then the set points for the two linear motors, moving the contact points, and controlling lateral motion and yaw. The kinematic state is also used for the visualisation. In this way, the natural lateral dynamics of the bicycle, including the rider, are preserved and act as in riding on the open road.

Bicycle model

A forward-moving bicycle can be balanced by steering into the undesired fall [23]. On the bicycle simulator, we can balance by laterally moving the two-wheel contact points. The input is then the forward speed and the steering angle and the output the lateral motion of the contact points. The model we use for that is the so-called Carvallo–Whipple bicycle model as presented in the bicycle benchmark paper [24]. This is a three-degree-of-freedom rigid bicycle/rider model with idealised knife-edge rolling contact with zero lateral slip at the contact points. The state of the bicycle, see Figure 2, is defined by the lateral positions of the rear contact points, x_O, the yaw angle ψ of the rear frame about the vertical axis, the roll angle θ of the rear frame about the line of contact, the steer angle δ of the front frame with respect to the rear frame, and the forward speed v_R. The linearised state equations which describe the rate of change in the lateral position of the rear and front wheel contact

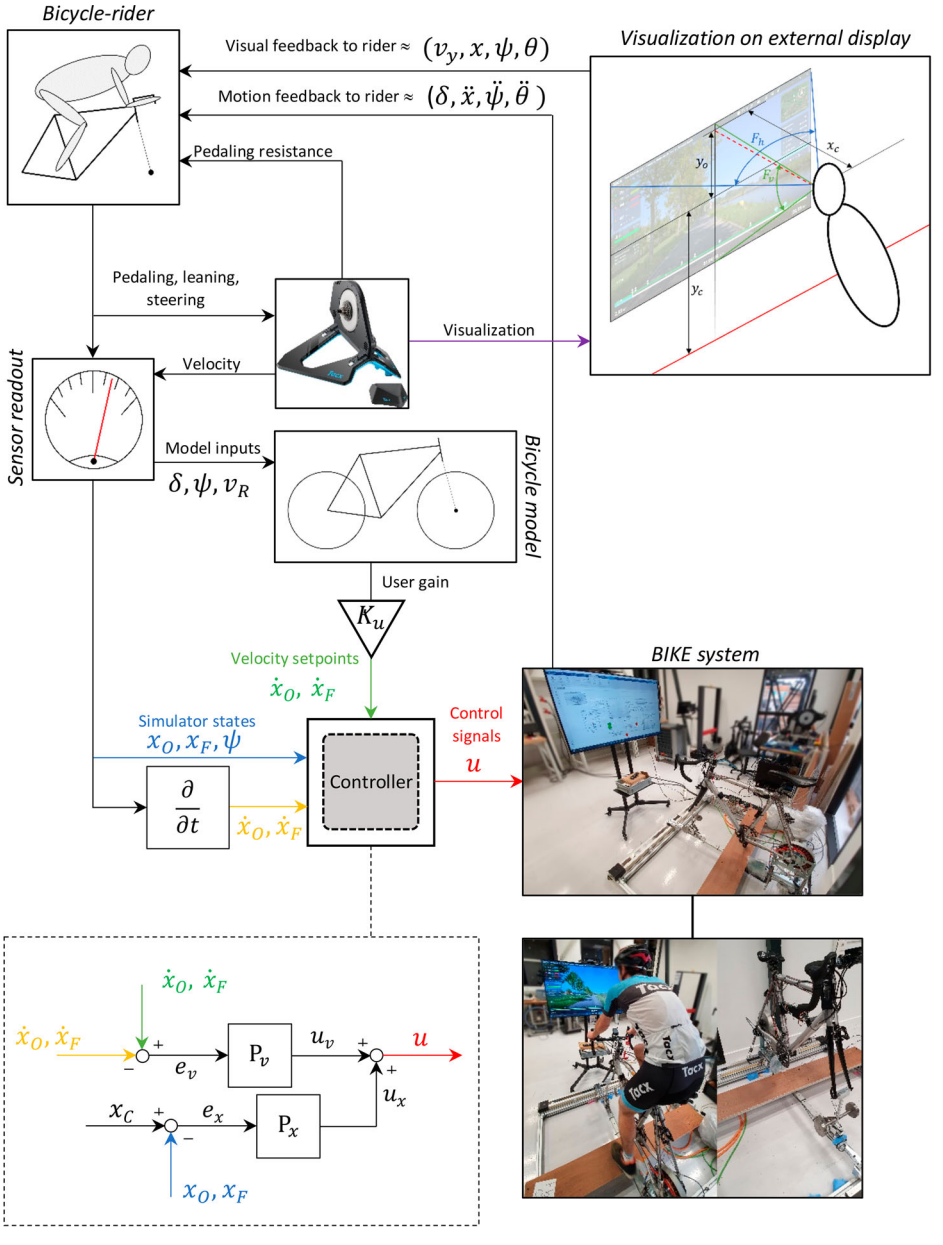

Figure 1. Layout of the bicycle simulator setup together with the basic control scheme for the linear motors moving the rear and front contact points x_O and x_F. The state of the bicycle is defined by the rear frame roll angle θ, the steering angle δ, the forward speed v_R, and the lateral positions of the rear and front wheel contact point, x_O and x_F, which determine the lateral position of the bicycle and the heading ψ, see also Figure 2. The visualisation is a prerecorded video with speed control, depending on the rider's velocity.

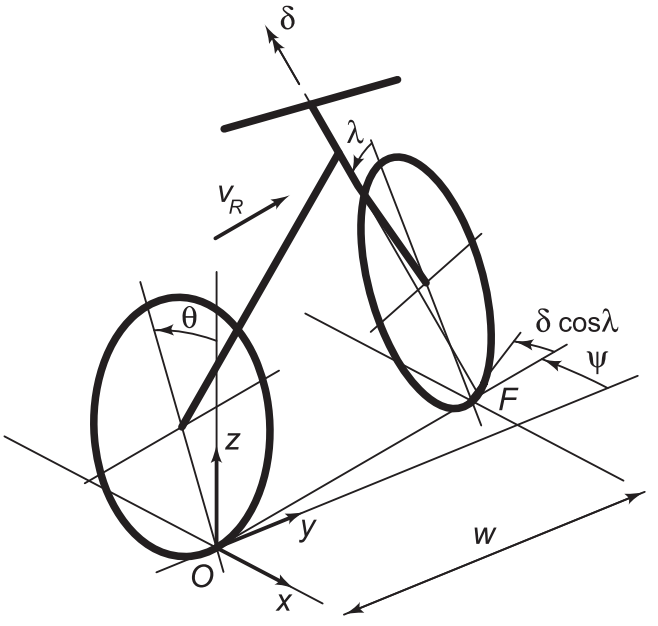

Figure 2. Bicycle model used for the simulator control setup. The bicycle has a wheelbase w and a tilt of the steering axis λ. The state of the bicycle is defined by the rear frame roll angle θ, the steering angle δ, the forward speed v_R, and the lateral positions of the rear and front wheel contact point, x_O and x_F, which determine the lateral position of the bicycle and the heading ψ.

Figure 3. Bicycle simulator mechanical setup. The visualisation screen, the used bicycle frame and the electromechanical system are visible. Springs at the rear of the bicycle keep the bicycle in its upright position, and a mass-spring combination at the front of the bicycle provides steering resistance to the user.

points are,

$$\dot{x}_O = -v_R \psi, \tag{1}$$

$$\dot{x}_F = -v_R(\psi + \delta \cos \lambda). \tag{2}$$

Here λ is the steering axis tilt with respect to the vertical such that the ground projected steering angle is $\delta \cos \lambda$. These state equations are linearised about the straight ahead upright position and are to the first order independent of the rear frame roll angle θ. The heading of the bicycle can be calculated to the first order from,

$$\psi = (x_O - x_F)/w, \tag{3}$$

with the constant wheelbase w. These three equations determine the required velocity of the two linear motors moving the contact points.

Motion cueing

Data recording and motion control is structured as in Figure 1. A hardware controller (see Figure 1) enacts the bicycle model, to generate lateral velocity and position set-points for both the rear and front linear motor. Motions are constrained within the operating range of the simulator using a washout filter, and controlled with a dual P-controller of the actuator velocity and position as a return-to-zero enforcer. The latter acts on the displacement between an arbitrary (x_C) and measured position of either point O or F (see Figure 2 for definitions). Thus the bike path is actuated directly as is common in motion base simulators. The bike roll motion is not actuated and is only supported by a weak spring to stabilise the stationary bike without rider. During cycling the rider stabilises the roll motion exactly like in real cycling, by steering into the undesired fall [23]. The contact point of the wheels are then brought back under rider by the linear motors, controlled by the bicycle kinematics model.

Electromechanical design

The mounted bicycle is connected to a resistance unit (a disassembled Tacx Neo 2T indoor trainer, functioning as a standalone braking unit), which applies braking power related to the user's pedalling power and rear-wheel velocity, providing a sense of velocity to the user and requiring a realistic effort from the user. The twin-railed actuator configuration was picked for its independent controllability, should individual augmentations need to be made to only the front or rear actuator. Pilot measurements combined with the maximum allowed rider mass requirement of 120 kg prescribed the minimum actuator performance in terms of force, acceleration and velocity. A design safety factor of approximately 2.3 was used for the lateral force.

The actuators which were picked based on the force-acceleration requirements are a set of Parker OSPE32BHD linear positioners [25].

Beneath the front fork support, a linear guide is used to allow bicycles with different wheelbases to be mounted. The front wheel contact support is a complete analogue to the real bicycle, with a heading angle and a trail, such that the front wheel contact force is transmitted in a correct way to the steering torque. However, the front wheel is not present,

which means that part of the inertia and the gyroscopic effect of a rotating wheel, are missing. Usually the gyroscopic effect of the front wheel is only a small contribution to the steer torque [23]. Therefore, we only added the missing inertia and a spring to generate some additional steering stiffness. All users were able to control the simulator with this steering setup. Another set of springs at the rear of the bicycle keep it upright without a rider and compensate for the weight of the resistance unit, but only just, to minimise interference with the rolling behaviour of the user. At rest, a slight roll angle of $\theta \approx 5^o$ is sufficient to knock it over its balancing point.

The BIKE model was implemented with the direct measurement of steer angle δ and the roll angle θ with potentiometer rotation sensors. Conveniently, the resistance unit uses permanent magnets in its rotor, of which the change in magnetic field can be measured with a HALL-sensor. Thus, a direct measurement of the rear-wheel velocity v_R is available as well. All sensor signals are filtered, using low-pass filters of different passbands frequencies and order, optimising the trade-off between remaining signal noise and filter group delay.

With this augmentation, the control algorithm was implemented using National Instruments PCIe-6353 I/O hardware, running on MATLAB Version 2020b on a Dell Precision 5820 workstation. This workstation uses an Intel i9-10920X 12-core CPU and 128GB of DDR4 RAM. Using MATLAB's SIMULINK Desktop Real-Time extension, real-time, high-speed communication with the hardware is possible.

A separate control system is attached to each of the two actuators which takes an analogue voltage input and uses that as a motor velocity setpoint. This input signal is sampled by this control system at 16 kHz. The limiting factor in the control loop is the MATLAB control loop execution, which limits the system bandwidth to 100 Hz. The BIKE system has several safety features built-in, both hardware and software, to guarantee the safety of its users. A hardware dead man's switch was attached to the user's wrist, cutting power if that switch were opened for any reason. The actuator system was configured in software in such a way that when either a bicycle roll or horizontal position threshold were crossed, the actuators would stop immediately. Moreover, the participants were instructed that they had the freedom to stop the experiment at any time, for any reason.

Visualisation

A component of the full system loop that needs to be emphasised is the visual system, due to its potential influence on the usability of the simulator. To mimic a visual environment experienced by the participants of this study outdoors, we use a visualisation system displaying prerecorded environments. The Taxc visualisation software [26] was selected for its availability, its resemblance to the outdoor experimentation environment and its ease of application with the used propulsion resistance unit. We use this to visualise the road on a large monitor. Screen-based visualisation, rather than head mounted, was selected for ease of use in particular when starting from standstill, and to prevent motion sickness [27]. More abstract, third-person options exist, e.g. [3], but were not explored in this study. The screen [1], is placed centred with the linear actuators. The middle of the screen is at $y_c = 1.29$ m from point Q, vertically. The participants' eyes are offset with $y_o = 0.32$ m vertically, $x_c = 1.09$ m horizontally. This creates a horizontal field of view of $F_h = 58.8^\circ$ (when the participant is centred with the middle of the screen), and a vertical field of view of $F_v = 33.3^\circ$, rotated downwards approximately 15.9° with respect to the horizontal plane.

Table 1. Participant demographics (mean ± standard deviation).

			Cycling Experience		
Number of participants	Age	Sex	Indoors	Outdoors	Mass
16	26.06 ± 4.234 yr	15M, 1F	1,375 ± 719 km/yr	2,688 ± 1,250 km/yr	81.97 ± 13.71 kg

The visualisation of the road on the display is stationary in lateral, vertical, roll, pitch, and yaw. Only longitudinal motion is visually presented, and this results in the bike moving forward in the visual environment. The display and thereby the visual road do not roll. Instead, the bicycle and the rider do roll, creating a full perception of roll through visual and vestibular cues. Likewise platform and rider move laterally and rotate in yaw, resulting in lateral and yaw motion relative to the display and thereby relative to the road.

Experimental validation methods

The simulator was experimentally validated using objective measurements of the bicycle motion and subjective user experience metrics.

Participants

15 participants were invited based on outdoor and indoor cycling experience, as well as availability both in and outside the company, since it has been shown that cyclists control bicycles differently based on experience [28]. Cycling experience is categorised with the yearly average distance travelled on any bicycle. The participants were not compensated for the experiment, and their personal data (age, gender, bicycle type, cyclist experience) were pseudonymised. Table 1 represents the subject demographics.

Experiment procedure

As summarised in Figure 4 data is collected in three main cycling configurations:

- Outdoor cycling, on a straight, asphalt road with no obstructions and sufficient road length, on an instrumented bicycle (Figure 5).
- The BIKE system from Figure 1 with full motion.
- A fixed setup based on the Tacx NEO 2T indoor bicycle trainer. Note that the visualisation with the fixed setup is as in the BIKE system, but now with no rider roll, yaw or lateral displacement.

Three manoeuvres were performed in the following order:

(1) Constant cycling on a straight, flat road at incrementally increasing velocities: 5, 10, 15, 20, 25, 30, 35, 40 km/h, while remaining seated on the bicycle for about one minute per velocity, not counting the acceleration time between velocities. Elapsed time and current velocity could be monitored by the cyclist on the Garmin Edge 530 device screen, or on the visualisation screen during indoor experiments.
(2) Zig-zagging at approximately 20 km/h, to obtain information on evasion manoeuvring and cornering. The maximum width of the motion is 1 m, to remain within simulator bounds. This width is indicated to the participant as the half-width of the road where

	Participant introduction	10 min.	Fill out IC form. Explain experiment procedures. Verify empty pedals.
Outdoor experiments	Prepare bicycle	5 min.	Startup RPi. Connect pedals. Fill out Q-forms
	Go-to outdoor experiment loc.	10 min.	Ride to experiment location.
	Outdoor experiments	14 min.	Start RPi meas. Start pedal meas. Calibrate pedals
	8 velocities	10 min.	5, 10, ..., 40 km/h straight
	Zig-zag	2 min.	Appr. 20 km/h, 1 m width
	Stand-up sprint	2 min.	No max. velocity
	Return ride	10 min.	Fill out Q-forms Stop RPi meas. Stop pedal meas.
Bicycle sim. experiments	Prepare bicycle	15 min.	Fill out Q-forms Change pedals. Start download pedals. Prepare bicycle sim.
	Bicycle simulator experiments	25 min.	Fill out Q-forms Start RPi meas. Start pedal meas. Calibrate pedals
	Accustomization	10 min.	80% sim. accuracy
	8 velocities	10 min.	5, 10, ..., 40 km/h straight
	Zig-zag	2 min.	Appr. 20 km/h, 1 m width
	Stand-up sprint	2 min.	No max. velocity (opt.)
Static sim. experiments	Prepare bicycle	15 min.	Fill out Q-forms Change pedals. Start download pedals. Prepare static sim.
	Static simulator experiments	15 min.	Start RPi meas. Start pedal meas.
	8 velocities	10 min.	5, 10, ..., 40 km/h straight
	Stand-up sprint	2 min.	No max. velocity
	Experiment roundup	15 min.	Fill out Q-forms Fill out Q-forms +15 min.

Figure 4. Full experimental procedures with a short description of each experimental phase. Denoted are the outdoor, simulator with motion and static simulator measurement phases, as well as manoeuvres and actions.

Figure 5. Custom racing bicycle used for outdoor experiments. Includes the kinematics measurement board in the centre of the frame. Magnets in the rear wheel are used for velocity measurements. Saddle is adjustable for participants.

tests are conducted. This manoeuvre is not performed on the static setup, due to the impossibility of steering and controlling the bicycle.

(3) A standing-up cycling sprint, with no required velocity, other than that the subject should be able to maintain the velocity he picks for standing-up cycling for one minute.

Measurement of bicycle states

The bicycle used is an aluminium racing bicycle (Figure 5). The measurement system for collecting bicycle orientation and kinematics data is largely based on existing iterations of such a system [29–35], with the omission of steer-torque measurements and addition of crank torque, crank velocity and crank rotation angle measurements. The measurement system, transferable between bicycles, uses off-the-shelf components to remotely measure the bicycle's states. The sensors, and the respective data they produce, are enumerated below:

(1) Two 6-axis Inertial Measurement Units (IMU's), which measure acceleration and angular rates in a 3D coordinate system ($\vec{\mathbf{a}}_{I,r}, \vec{\mathbf{a}}_{I,f}, \vec{\boldsymbol{\omega}}_{I,r}, \vec{\boldsymbol{\omega}}_{I,f}$, subscripts indicating rear and front IMU's). The IMU's are located at the red squares in Figure 6.

The analysis applies a custom, complementary filter-based algorithm to compose the pitch, roll and yaw angles of the bicycle frame.

(2) One measurement potentiometer, which measures the steering angle of the bicycle front frame (δ).

(3) One Hall-effect sensor, which detects changes in magnetic field caused by magnets fixed to a bicycle wheel's spokes, which in turn can be turned into a velocity measurement (v_R).

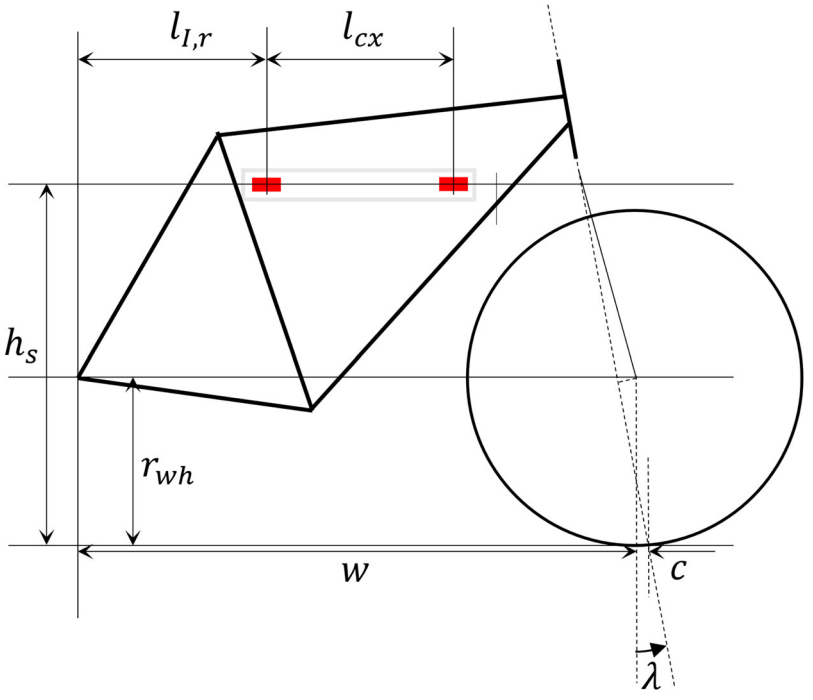

Figure 6. IMU placement on the bicycle, as red squares. Oriented with one measurement axis aligned with gravity, when bicycle is level. Relevant base bicycle and placement dimensions given, as well.

(4) One set of Garmin Rally 200 measurement pedals, which, in a specific debugging configuration, record raw pedal angular acceleration, angular velocity, crank angle and pedal force values (both tangential and radial) ($\alpha_T, \omega_T, \theta_T, F_{tan}, F_{rad}$).

Frequency domain analysis

In addition to a time domain comparison, frequency domain system identification is used to compare the dynamic interaction of the rider with the bicycle and the simulators.

The comparison between datasets, recorded for a certain participant performing a certain cycling manoeuvre, is based on the fit of the kinematic data to an LTI state-space model. Such a method has been applied before and has been shown to be a fairly accurate method of representing bicycle-rider dynamics, even with limited model degrees of freedom [29]. When a model has been obtained for a certain manoeuvre, comparison between different riders and other manoeuvres is simplified. Furthermore, if the measured kinematic data fits well within the confines of predefined models derived from bicycle geometry, this is another indication that the applied bicycle model in the simulator is sound. At the very least, a fit of data to a certain predefined model should reduce noise in the resulting frequency response.

In this study, particular interest lies with the lateral dynamics of a bicycle and with steer-to-roll dynamics. Therefore, two models are defined as in Table 2.

The state-space representations of the models are pre-estimated based on geometric relations in a bicycle before fitting the data using Matlab's SSEST function, based on

Table 2. Input and output signals for the system identification of intrinsic bicycle-rider kinematics.

Parameter	I/O	Description	Unit	State-space model
δ	Input	Steering angle	[*rad*]	Lateral dynamics
a_x	Output	Lateral acceleration point *O*	[m/s^2]	Lateral dynamics
$\dot{\psi}$	Output	Yaw rate	[rad/s]	Lateral dynamics
δ	Input	Steering angle	[*rad*]	Steer-to-roll dynamics
T_{roll}	Input	Roll torque	[*Nm*]	Steer-to-roll dynamics
θ	Output	Bicycle roll angle	[*rad*]	Steer-to-roll dynamics

Note: See Figure 2 for relevant coordinate system definitions.

mathematics proposed in Ref. [36]. For a discrete-time system, models take the shape of:

$$\begin{aligned}\mathbf{x}(kT_s + T_s) &= \mathbf{A}\mathbf{x}(kT_s) + \mathbf{B}\mathbf{u}(kT_s) + \mathbf{K}\mathbf{e}(kT_s)\\ \mathbf{y}(kT_s) &= \mathbf{C}\mathbf{x}(kT_s) + \mathbf{D}\mathbf{u}(kT_s) + \mathbf{e}(kT_s)\end{aligned} \tag{4}$$

These pre-estimated models, with to-be identified coefficients selected to fit to either the measured lateral or steer-to-lean dynamics, are:

- **Lateral dynamics model**: approximated as a two-dimensional model, where a certain steer angle scales with velocity to result in a certain lateral acceleration and yaw rate.

$$\begin{bmatrix} a_x \\ \dot{\psi} \end{bmatrix}_{k+1} = \begin{bmatrix} A_{a_x a_x} & A_{a_x \dot{\psi}} \\ 0 & A_{\dot{\psi}\dot{\psi}} \end{bmatrix} \begin{bmatrix} a_x \\ \dot{\psi} \end{bmatrix}_k + \begin{bmatrix} B_{a_x \delta} \\ B_{\dot{\psi}\delta} \end{bmatrix} [\delta]_k \tag{5}$$

$$\begin{bmatrix} a_x \\ \dot{\psi} \end{bmatrix}_k = \begin{bmatrix} 1 & 0 \\ 0 & 1 \end{bmatrix} \begin{bmatrix} a_x \\ \dot{\psi} \end{bmatrix}_k \tag{6}$$

  The identifiable parameters of the **A**-matrix are initially set to zero, except $A_{a_x \dot{\psi}} = -v_R$ due to an expected relation between the forward velocity, sideways acceleration and the bicycle's yaw rate. All unknown parameters of the **B**-matrix are initialised at zero, except for $B_{\dot{\psi}\delta}$, which is initially set equal to $\frac{v_R}{w} c \cos(\lambda)$. Both non-zero initialisation parameters are based on the linearised (derivative of) the derived bicycle model applied in the simulator.
- **Steer-to-roll dynamics**: approximated as a one-dimensional model, where a certain steering angle and roll torque result in a certain bicycle roll angle.

$$[\theta]_{k+1} = [A_{\theta\theta}][\theta]_k + \begin{bmatrix} B_{\theta\delta} & B_{\theta T_{roll}} \end{bmatrix} \begin{bmatrix} \delta \\ T_{roll} \end{bmatrix}_k \tag{7}$$

$$[\theta]_k = [1][\theta]_k \tag{8}$$

  All steer-roll parameters are initialised equal to zero. In the measurements of δ and θ, a phase delay seemed to exist between them, which scaled with the forward velocity of the bicycle. The state-space algorithm is therefore also initialised with an (empirically determined) input delay of $(-\frac{1}{0.0038 v_R^{1.25}} - 35.12) T_s$ seconds.

All recorded datasets are truncated where the bicycle velocity is approximately constant for the duration of the manoeuvre. All inputs and outputs, for both state-space models, are de-trended linearly over a certain manoeuvre window, to remove drift or offset effects as

well as improve the state-space estimation accuracy. This is considered justified with the notion that higher-frequency signal content ($>$ 0.1 Hz, observed from these and previous experiments) relates to the balancing kinematics of the bicycle-rider system, thus we are not interested in very low-frequency ($<$ 0.1 Hz) content (since control actions in that frequency range cannot be reproduced on the simulator). Input and output signals are always visually inspected before the derived signals and systems are approximated, to verify the effect of the above operations. Bad or incomplete data are omitted from results.

Apart from frequency responses, the frequency-dependent coherences are computed based on the in- and outputs of Table 2 and used to filter the date used in frequency response functions. The upper passband frequency of the low-pass filter is equal to 1.5 times the frequency where the coherence first rises above 0.7 (sweeping the frequency from low to high). Coherence was derived through Matlab's MSCOHERE function.

Subjective measurements of simulator fidelity

In order to evaluate what cyclists experience as realistic cycling and to find out whether the bicycle simulator was disruptive compared to their usual outdoor cycling experience as well as an improvement over static cycling, a number of questions have been asked. The possible answers consist of a score between 1 and 10, whole numbers only. The questions are presented to the participant at the start of all experiments, for the subject to keep in mind during the experiments, and answered at different times.

The questions asked are subdivided into two categories; questions related to the current experiment and questions specifically touching upon differences between the simulator and outdoor cycling. Questions of the first category are asked after every cycling experiment; outdoor, simulator and fixed setup (Table 3).

Questions of the second category, which compare different situations or are specific to the BIKE system are answered after all experiments are completed (Table 4).

Table 3. Subjective questionnaire for the participants with questions pertaining to each cycling situation (outdoor, simulator and static).

	Question	Cat.
Q1	I felt like I was riding a bicycle	CR
Q2	I felt like I was riding *my* bicycle	CR
Q3	Steering felt natural during the ride	CR
Q4	Maintaining control of the bicycle was effortless	CR
Q5	Balancing the bicycle felt natural during the ride	CR
Q6	I felt I was not restricted in rolling the bicycle beneath me	CR
Q7	The forward motion I experienced felt coupled to my pedalling cadence and power	CR
Q8	I was focused more on the mechanical aspects and limitations of the bicycle, than on the actual cycling	CR
Q9	The velocity I was cycling at felt the same as the velocity of what I was seeing	VIS
Q10	I felt like I could ride the bike wherever I wanted on the road that I could see	VIS
Q11	I felt like I was in control of the bicycle	CC
Q12	I felt comfortable during cycling	CC
Q13	I felt safe during the ride	CC
Q14	The ride was enjoyable	CC
Q15	During cycling, I felt as if there was some aspect of cycling missing. If scored above 1, this was missing in my view:	CC

Notes: Scored from 1 (complete disagreement) through 10 (complete agreement), whole numbers only. Questions are asked only at the end of every cycling situation. Questions related to Cycling Realism (CR), Visualisation (VIS) and Controllability & Comfort (CC).

Table 4. Subjective questionnaire for the participants with questions specifically comparing certain aspects between cycling experiments.

	Question
C1	Balancing cost more effort on the simulator than outside
C2	Delivering pedalling power cost more effort on the simulator compared to outside
C3	Steering the bicycle had the same result on the simulator, as outside
C4	The sideways velocity of the simulator felt natural, compared to outside
C5	The physical motion of the simulator influenced my cycling positively
C6	The visualisation presented on the simulator influenced my cycling positively

Note: Scores from 1 through 10 are possible, whole numbers only. Questions are asked only after all experiments have been conducted.

An additional metric evaluated with the simulator is simulator-induced motion sickness, or simulator sickness. Simulator sickness is a separate category which is based on the Simulator Sickness Questionnaire (SSQ) method proposed by Kennedy & Lane [37]. This method is widely applied in studies on simulator sickness occurring in vehicle simulators, for example in Refs [38–40], thus it is applied here as well. What is important to note is that in the simulator presented in this study, physical exertion is a large part of the usage of the simulator, so results from the statistical scores have been interpreted accordingly.

What we expect for the incidence of simulator sickness, is that simulator sickness incidence can increase going from outdoor to indoor cycling experiments, but that the incidence remains small among participants. This is due to the use of an external monitor, as well as due to cycling being a high-involvement activity. Balancing and controlling a bicycle costs effort, which requires one's concentration and focus. Increased effort and focus on a certain controlling task have been shown to decrease simulator sickness incidence [40–42].

Results

All participants were able to perform almost all manoeuvres on the bicycle outdoors, the BIKE simulator with motion and the fixed simulator. Participants seemed to cope well with the BIKE system as a whole. All participants were able to get used to the simulator's motion response within a reasonable amount of time, where the person who struggled most took approximately ten minutes to start up from standstill, and another ten minutes to relax and use the simulator as intended.

During experiments, three participants were not able to reach the prescribed velocity of 40 km/h on the road due to the high required effort involved (participants 008, 010 and 015). Only one participant (008) was not able to perform higher-velocity manoeuvres on the simulator due to the motions being too jittery and unstable for him to continue. Based on verbal feedback during the experiment and observations by the experiment supervisor, this was attributed to stress resulting in tension in the arms of the participant. This participant stated to have little experience with racing bicycles. Other participants, with more cycling experience, showed more relaxed behaviour on the simulator and did not experience instability problems at all. However, almost all participants showed difficulty with attaining the lowest velocity (5 km/h) on the simulator and performed the first manoeuvre at a slightly higher velocity.

Motion results from the fixed cycling simulator experiments are not reported, since they remain near-zero and seemingly uncorrelated across manoeuvres. The standing-up

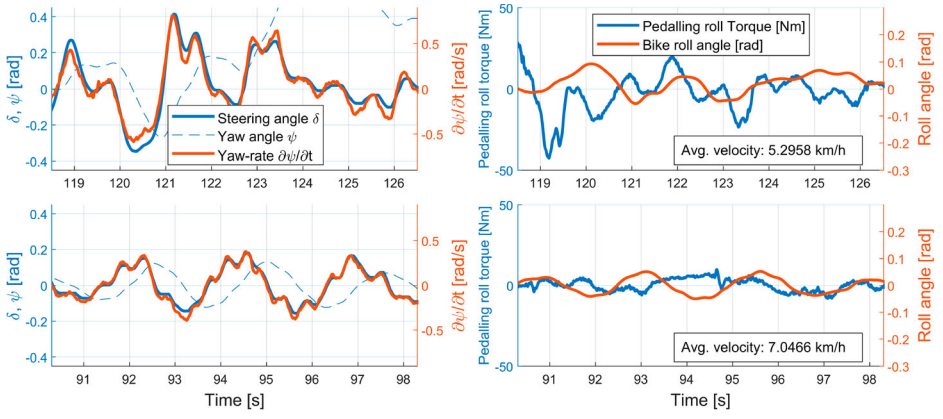

Figure 7. 5 km/h cycling in a straight line, during both outdoor cycling (top) and simulator cycling (bottom). Shown are Steering angle δ, yaw-rate $\dot{\psi}$ and yaw angle ψ (left) and bicycle pedalling roll torque and roll angle θ (right). Note the different y-axes and their scales.

manoeuvre was not performed on the simulator, since the behaviour of the simulator was experienced as too jittery while participants stood up from the saddle. Larger excitations of the steering angle during standing up, as well as an undamped steering response, may have been the cause of this instability.

It became clear that during the experiments, the focus of the participants lied with observing and acting on the speed reading on either the screen, the Edge device or the visualisation presented during indoor experiments. This should be taken into account while interpreting the subjective results.

Time-domain signals

Bicycle attitude and rider control signals recorded during the experiments give a first insight in the performance of the simulator compared to outdoor cycling. Figures 7–10 show a sample of time-domain signals from various participants, for several straight-line speeds and a zig-zagging manoeuvre. We are interested in seeing the different responses of the simulator with respect to common inputs. We present steering angle δ and the resulting yaw angle and yaw rate (left) as well as the roll torque resulting from left-right pedalling cadence and the resulting roll (right). Pedalling roll torque was derived from pedal force assuming a fixed moment arm equal to the lateral position of the pedal centre.

These figures show a general similarity in signal amplitude between bicycle and simulator. The relation between steering angle and yaw-rate seems to generally be similar, too. The relation between steering angle δ and yaw-rate $\dot{\psi}$ scales with forward velocity, which is in accordance with our and existing models. Pedalling roll torque does not appear to scale with increasing forward velocity, but this torque also depends on the gear ratio of the bicycle. So discrepancies in torque between velocities and outdoor or simulator cycling are not unexpected.

Higher speeds show qualitative correspondence of simulator and bicycle data where steer and roll angle are aligned in time indicating adequate steering to achieve a balanced

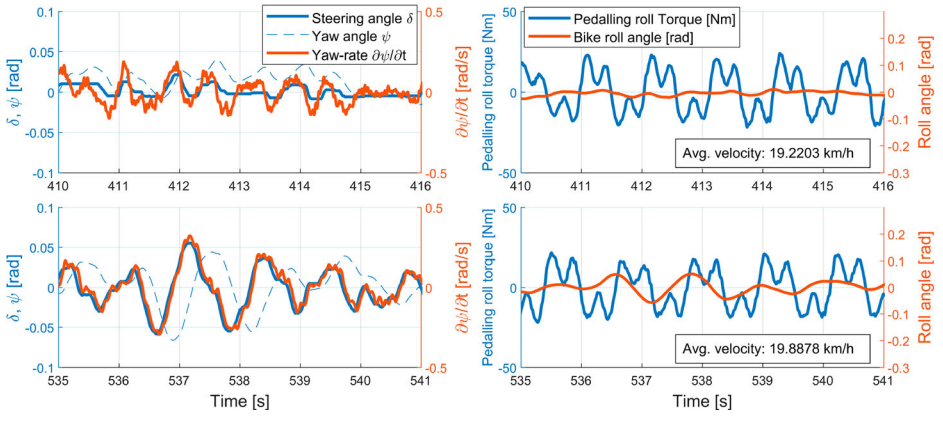

Figure 8. 20 km/h cycling in a straight line, during both outdoor cycling (top) and simulator cycling (bottom). Shown are Steering angle δ, yaw-rate $\dot{\psi}$ and yaw angle ψ (left) and bicycle pedalling roll torque and roll angle θ (right). Note the different y-axes and their scales.

cycling state. During low-speed straight-line cycling (Figure 7) large steering angles are observed associated with the challenge to balance at lower speed.

However, the steering sensor expresses some plateauing behaviour, in particular at 40 km/h. This behaviour may be caused by one or a combination of the following three phenomena. Firstly, with increasing bicycle velocity, a smaller steering action is required for the same lateral displacement. Thus, at 40 km/h, very little steering control is required for balance correction. Secondly, there was some mechanical play in the transmission between the handlebar stem and the rotation sensor, due to the use of a toothed belt. And finally, the conversion from analogue to digital only allows for a certain limited signal precision between conversion steps, further amplifying signal plateauing. Signal noise is more prevalent in all sensors outdoors due to road contact vibrations.

Input–output phase delays seem to start occurring with increasing forward velocity. From visual inspection (Figure 8) shows a slight delay between an applied steer angle and the resulting yaw-rate. This delay becomes more apparent during high-velocity cycling (Figure 9). This delay, likely to be introduced by the electromechanical system, is apparent with all participants. We do not observe this delay during the same manoeuvre performed outdoors. A frequency domain analysis should provide more information on this phenomenon across all participants.

Frequency domain analysis

We expect the frequency of balancing control actions by the cyclist to be closely tied to the pedalling frequency, as has been observed in earlier studies [18]. Thus, very low (< 0.1 Hz) and high (> 2 Hz) frequency dynamics are beyond our scope of interest. Figure 11 shows the directly-obtained frequency response between relevant inputs and outputs for outdoor and simulator cycling. The fitted state-space model is also shown. This particular analysis is obtained from a straight-line section at a constant velocity of 20 km/h. Gains for a_x and $\dot{\psi}$, from this point on, are normalised with v_R^2 and v_R, respectively. This allows for a

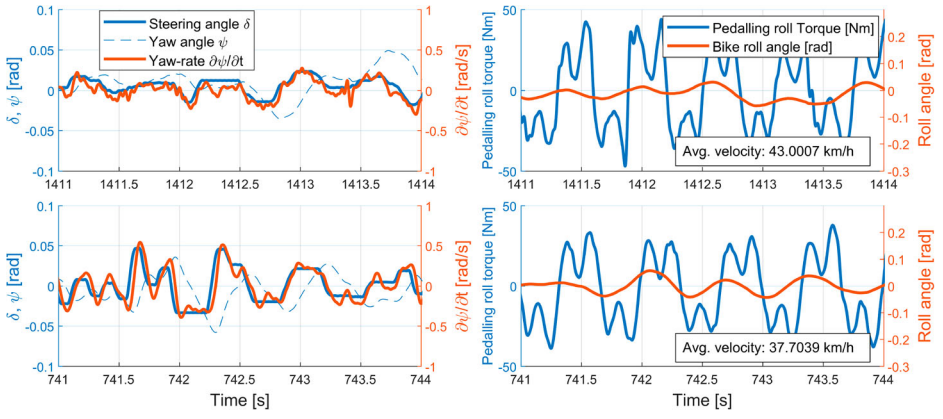

Figure 9. 40 km/h cycling in a straight line, during both outdoor cycling (top) and simulator cycling (bottom). Shown are Steering angle δ, yaw-rate $\dot{\psi}$ and yaw angle ψ (left) and bicycle pedalling roll torque and roll angle θ (right). Note the different y-axes and their scales.

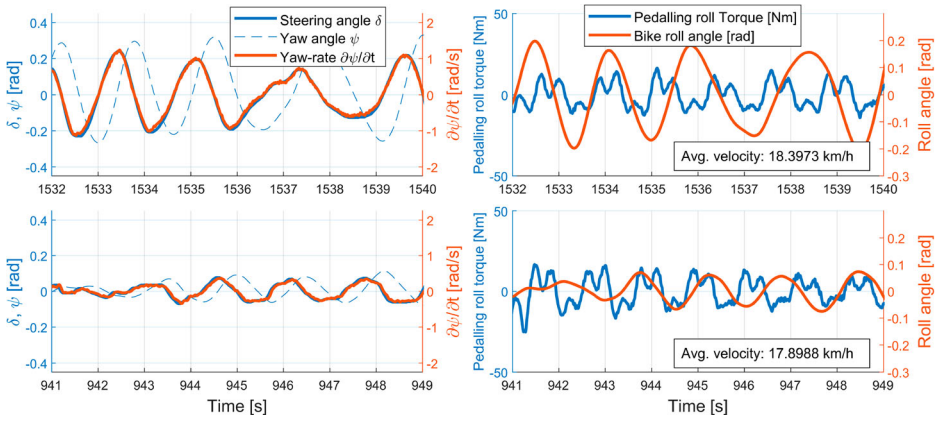

Figure 10. Zig-zagging at approximately 20 km/h, during both outdoor cycling (top) and simulator cycling (bottom). Shown are Steering angle δ, yaw-rate $\dot{\psi}$ and yaw angle ψ (left) and bicycle pedalling roll torque and roll angle θ (right). Note the different y-axes and their scales.

condensed qualitative comparison between velocities and manoeuvres. v_R is taken as the average velocity of a certain windowed dataset.

All fitted state-space models produced a linear gain-frequency relation over the frequency range of interest (and the frequency-dependent coherence is very high in this range). To give a comprehensive overview of differences between outdoor and simulator-fitted state-space responses, the average gain for each input–output relation was extracted from the frequency response between half and double the cyclist's pedalling frequency of a certain manoeuvre. This increases robustness of the following comparison. Phase values were extracted exactly at cadence frequency.

Figure 12 shows the condensed model fit parameters of the full set of lateral input–output relations: δ to a_x and $\dot{\psi}$, in terms of average gain and phase. Figure 13 shows the relation between steering angle δ, roll torque and the resulting lean angle θ. Model fits

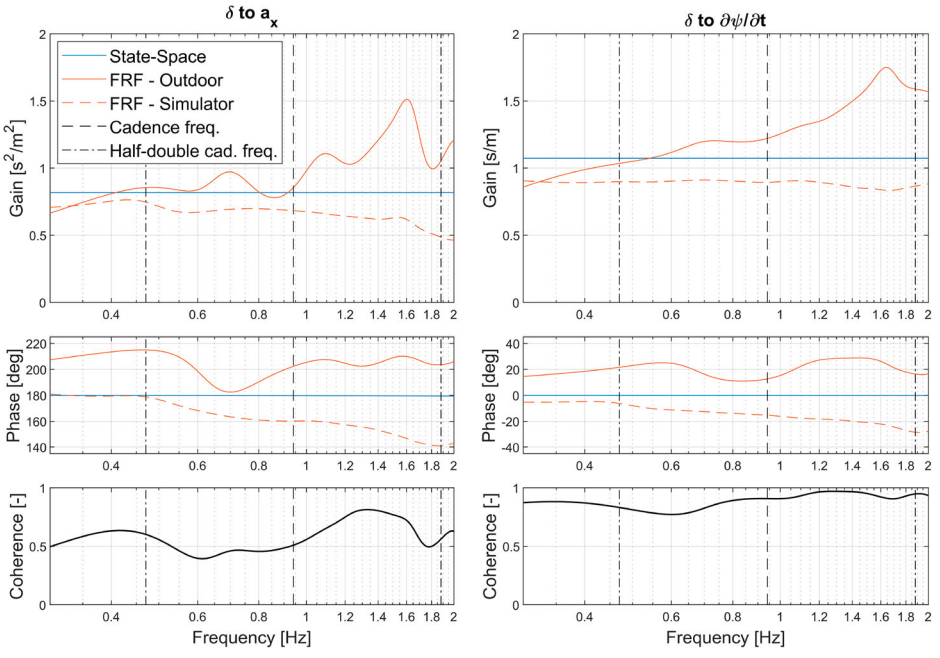

Figure 11. Straight-line, 20 km/h frequency response of the lateral dynamics during outdoor and simulator cycling. The relation between input steering angle δ and velocity-normalised lateral acceleration a_x (left column in figure) and yaw-rate $\dot{\psi}$ (right column in figure) are shown in terms of gain, phase and coherence. Both the fitted state-space response and directly-obtained frequency response are shown. The participant's cadence frequency is indicated with a vertical dashed line, and its halve and double are indicated with vertical dash-dot lines.

which produced a 20% or worse reproduction of original input data are omitted from these results. Boxplots show the grouping of gains from participants. Resulting phase responses are wrapped with steps of 360°. Bold-faced boxes indicate a p-value smaller than 0.05 when the distributions for a certain manoeuvre between outdoor and simulator cycling are compared based on a two-sided t-test . In this analysis, the fixed cycling setup is omitted since no steering was performed. We observe again what was seen in the time-domain analysis. The gains related to steering input and lateral outputs, between outdoor and simulator cycling, do not differ significantly for any velocity. However, observing the trend suggests that an outdoor bicycle experiences a non-linear decrease in its dependency of a_x on velocity above 20 km/h, whereas the simulator – as its vehicle model dictates – behaves more constantly with increasing velocity. This is also the case for $\dot{\psi}$.

It appears that the largest differences between the simulator and outdoor cycling become evident when considering the phase. Almost all manoeuvres show a significant phase delay of the simulator response with respect to outdoor cycling as a result of an input δ. For $\dot{\psi}$, a phase delay during outdoor cycling is immediately present (albeit smaller), which also increases with increasing velocity.

For the model describing steer-to-roll dynamics, gain and phase metrics are computed from fitted state-space models (under the same conditions as the lateral metrics in Figure 12) and shown in Figure 13.

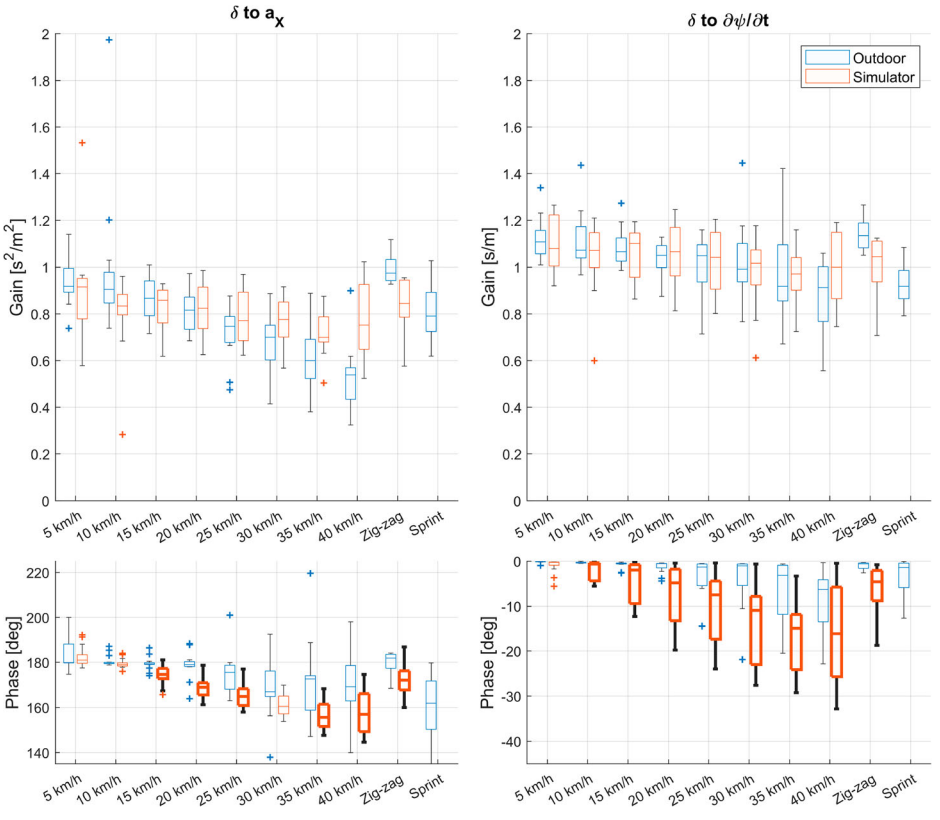

Figure 12. Condensed state-space frequency response parameters for lateral-based motion. Input steering angle δ is related to outputs lateral acceleration a_x (left) and yaw-rate $\dot{\psi}$ (right). Note that gains are normalised with velocity and the changing units on the vertical axes. Outdoor cycling (blue) and simulator cycling (red) are shown. Boldfaced boxes indicate a significantly ($\alpha < 0.05$) different distribution between outdoor and simulator cycling.

We observe that the steer-roll relations, comparing outdoor and simulator results, are relatively similar in terms of gain, although the gains observed on the simulator are somewhat lower and more closely grouped. The phase recorded for the steer-roll relation shows a relatively constant phase during outdoor cycling with increasing manoeuvre velocity, whereas the phase of the bicycle simulator decreases with increasing velocity. This behaviour for phase is similar to what the lateral dynamics showed (see Figure 12). The phase on the roll torque is very widely distributed. Factors as a subject's pedalling strategy could heavily affect where the highest forces are applied in the cadence cycle, thus shifting the roll torque signal with respect to the lean angle.

Subjective analysis

Table 5 shows the separate assessment of outdoor cycling, the simulator with motion, and the fixed setup, with comparisons of means based on a two-sided two-test.

These results show several significant effects, where the motion-based simulator generally scores much better than the fixed setup, with the exception of control effort which

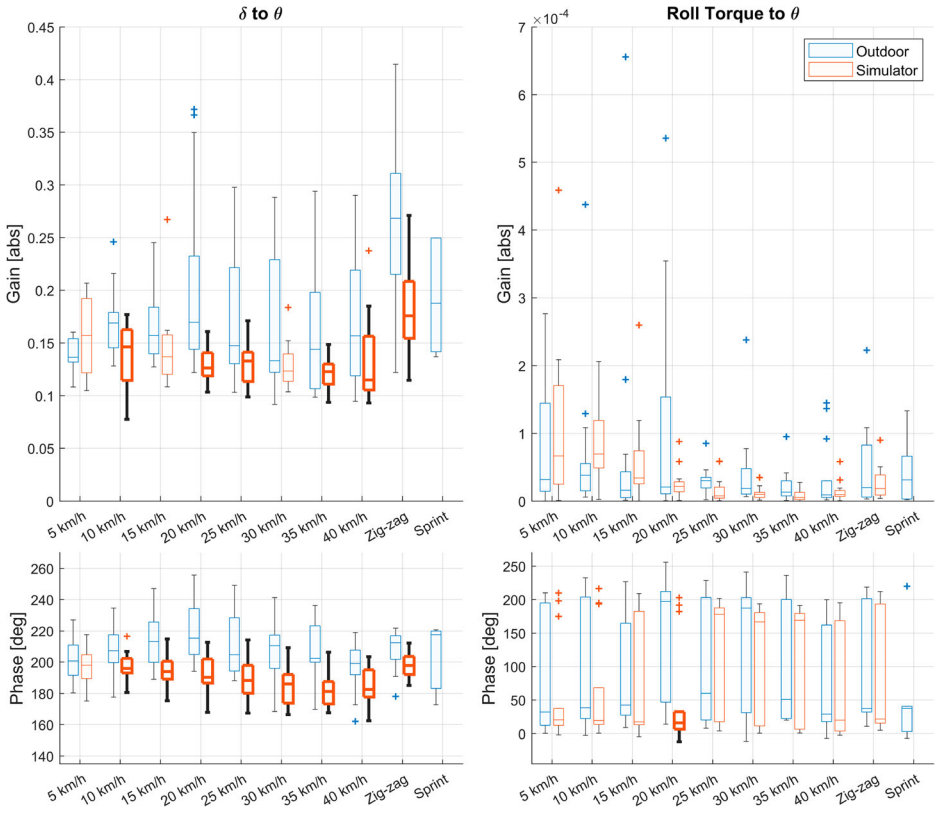

Figure 13. Condensed state-space frequency response parameters for lateral-based motion. Inputs steering angle δ (left) and pedalling roll torque (right) are related to a lean angle output θ. Outdoor cycling (blue) and simulator cycling (red) are shown. Boldfaced boxes indicate a significantly ($\alpha < 0.05$) different distribution between outdoor and simulator cycling.

was rated better with the fixed setup. The motion-based setup received positive ratings around 7 in many aspects with somewhat lower ratings for visual velocity (5.5) and visual manoeuvring (5.1).

The comparative questions asked after all experiments were conducted, also provide a rather positive evaluation of the motion-based simulator with a somewhat larger variation between participants (Table 6).

In terms of simulator sickness, participants showed no particular physical response to the combination of the visual system and the simulator. The highest scores on the SSQ spectrum were given during indoor cycling (either simulator or static setup) on the *fatigue* and *sweating* scores. After 15 minutes, the intensity of these (and other) symptoms usually reduced to the level the participants experienced 15 minutes before undertaking the experiment. See Table 7 for the scores given by participants, adapted for the usual 0 to 3 scoring range of the method described in Ref. [37].

Scores regarding simulator sickness remained low overall. The increased scores recorded directly after experiments are generally a result of increased sweating and fatigue scores due to the physical intensity of the experiment. The order of experiments (outdoor

Table 5. Subjective scores of questions per setup.

Question	Results (mean, std.) Outdoor μ_o, σ_o	Simulator μ_s, σ_s	Fixed μ_f, σ_f	Significance (p-value) Sim. vs. Out. $p_{o,s}$	Out. vs. Fixed $p_{o,f}$	Sim. vs. Fixed $p_{s,f}$
Felt like riding *a* bicycle?	10.00, 0.00	7.53, 1.13	5.67, 1.54	0.000	0.000	0.001
Felt like riding *my* bicycle?	6.50, 2.56	4.87, 2.13	3.87, 1.96	**0.072**	0.004	**0.192**
Did steering response feel natural?	9.00, 1.36	6.73, 1.67	1.20, 0.56	0.000	0.000	0.000
Maintaining control cost no effort?	9.21, 1.05	6.28, 1.81	9.79, 0.58	0.000	**0.086**	0.000
Did balancing the bicycle feel natural?	9.29, 0.99	6.92, 1.59	4.14, 3.23	0.000	0.000	0.008
Bicycle roll did not feel restricted.	9.79, 0.58	7.43, 2.24	4.38, 3.31	0.001	0.000	0.009
Pedalling and forward motion felt coupled.	9.57, 0.94	5.86, 2.60	3.50, 2.71	0.000	0.000	0.027
Focus lied with system rather than cycling.	3.36, 2.44	4.79, 2.58	2.57, 2.21	**0.144**	**0.380**	0.022
Visual velocity corresponded with expectation.	10.00, 0.00	5.50, 2.41	5.50, 2.82	0.000	0.000	**1.000**
Felt free to manoeuvre bicycle in visuals.	10.00, 0.00	5.13, 2.88	2.07, 2.34	0.000	0.000	0.003
Felt like I was in control of bicycle.	9.60, 0.74	7.27, 1.67	7.53, 3.31	0.000	0.026	**0.783**
Felt comfortable during cycling.	9.13, 1.06	7.13, 1.64	8.20, 1.57	0.001	**0.066**	**0.080**
Felt safe during cycling.	9.20, 1.61	7.53, 1.77	9.87, 0.52	0.012	**0.139**	0.000
The ride was enjoyable.	9.09, 1.04	7.73, 2.53	7.09, 1.64	**0.115**	0.003	**0.492**
Felt like something was missing.	1.07, 0.27	3.79, 1.58	6.07, 2.37	0.000	0.000	0.006

Notes: Shown *p*-values refer to a two-tailed t-test, comparing the means of simulator and static cycling question responses to the mean of the outdoors's. *P*-values higher than 0.05 are boldfaced. μ and σ indicate the mean and standard deviation of the response distribution. Subscripts refer to outdoor ($_o$), simulator with motion ($_s$) and fixed setup ($_f$).

Table 6. Subjective scores of questions comparing the motion-based setup to outdoor cycling.

Question	Results (mean, std.) μ, σ
Balancing cost more effort on simulator than outside.	5.80, 2.60
Delivering power cost more effort on simulator than outside.	3.00, 3.05
Steering on the simulator had the same result outside.	6.07, 2.15
Sideways velocity on simulator felt natural, compared to outside.	6.27, 1.71
Simulator motion influenced my cycling and balancing positively.	7.13, 2.33
Visualisation on simulator influenced my cycling and balancing positively.	6.47, 2.62

μ and σ indicate the mean and standard deviation of the response distribution.

to simulator to fixed) is recognised in the general increase in fatigue and sweating scores with changing experimental setups.

Discussion

The BIKE system is, for a subject pool of 15 participants, well-controllable and requires less than 15 minutes to get used to, in its current state. Users do not require preexisting experience with racing bicycles to be able to use this simulator, but cycling experience aids in the ease of getting used to the simulator (which was observed during experiments). This implies that the natural control behaviour that is usually applied to balance a bicycle laterally accelerating the support line of the bicycle beneath its user's centre of mass [20] is a viable method of controlling this simulator. Participants also subjectively rate the BIKE as being more realistic than the fixed setup.

While the recorded kinematics show a similar steering response between outdoor cycling and the BIKE system in terms of gain for lateral dynamics, the phase response clearly shows a difference, which is velocity-dependent. This is not unexpected, since delay is introduced through model, control and actuator dynamics. The current state-space

Table 7. Mean and standard deviations of Simulator Sickness Questionnaire scores entered by participants in three cycling situations.

	Time of recording	Nausea μ_N, σ_N	Oculomotor μ_O, σ_O	Disorientation μ_D, σ_D
Outdoors	-15 min	3.82, 5.59	5.86, 7.81	2.60, 5.52
	0 min (directly after)	21.88, 14.81	17.18, 14.34	4.08, 8.54
	+15 min	8.14, 14.63	7.48, 8.17	1.48, 4.45
Simulator	-15 min	5.34, 6.89	7.48, 8.01	1.86, 4.55
	0 min (directly after)	28.75, 12.89	17.99, 11.14	4.83, 7.55
	+15 min	8.65, 8.09	7.68, 8.64	2.23, 5.07
Static	-15 min	7.89, 8.59	7.48, 8.79	2.23, 5.07
	0 min (directly after)	32.05, 18.79	18.39, 15.48	3.71, 8.33
	+15 min	9.92, 10.28	9.10, 8.65	1.86, 4.55
Full range		200.34	159.18	250.56

Notes: Indicated are at what time the scores were recorded, and what the resulting sickness scores were. The three categories of SSQ (nausea, oculomotor and disorientation, $(_N)$, $(_O)$, $(_D)$, respectively) are represented as summed scores in this table. Highest possible scoring per SSQ category given at the bottom of the table.

model does not allow direct comparison to existing theoretical kinematic bicycle models or identified bicycle models from measurements ([24,43] or [29,30], respectively). Adapting experiments such that such a comparison is made easier may prove useful for further analysis of the dynamic accuracy of the BIKE system. Time-domain signals on bicycle roll, steer and yaw angles from existing experiments do, however, show the same order of magnitude for similar experiments [28,29,31,32,34].

Subjective scoring regarding the questionnaire on the experience of the simulator remains to be interpreted with care. It appears that the simulator subjectively performs much more comparable to outdoor cycling, as compared to the fixed setup, and that only in terms of enjoyment and sense of using their own bicycle, major differences remained. However, during experiments, participant's attention mainly lied with maintaining the required speed for a certain experiment, both according to the participants themselves and the author as an observer. Arguably, to obtain a conclusive answer on how the simulator performs subjectively, the experiment design should be altered in such a way that no focus of the participant is required for a certain manoeuvre. Questionnaire should then be focused on certain well-defined aspects of the simulator, rather than being broad and sometimes too open to interpretation.

As was the expectation based on previous studies on simulator sickness, no real incidence of it can be attributed to be a direct effect of the visualisation or physical motion applied in the simulator. The required physical effort is expected to be the cause of increased fatigue and sweating scores during experiments. Other aspects of simulator sickness remained low. As other studies have shown, a high-involvement task, such as balancing a bicycle, can also reduce the risk for simulator sickness [40–42]. A study [44] with a (static) bicycle ergometer and external monitor also investigated sickness effects, where more incidence of simulator sickness was recorded, but this setup did not include physical motion other than pedalling. Adding motion in a simulator, and letting that motion be similar to what one would expect (from a bicycle, in this case) also reduces simulator sickness incidence [45]. However, where there was no motion, i.e. with the static setup, no increase in simulator sickness incidence was observed. This could be due to the fact that participants were very focused on maintaining the correct velocity, or that they were not really immersed in the visual environment. The relatively short experiment duration could

have been a factor as well. Furthermore, a large field of view is required to induce a sense of immersion with the viewer (approximately 120°, [46]), increasing the risk for simulator sickness, but such a situation was not present in the bicycle simulator.

Conclusion

In this study, we set out to present a novel method of realistic bicycle simulation, present the BIKE simulator design and validate it using a range of objective and subjective measurements. With the BIKE simulator, a bicycle's natural motion is preserved, eliciting a realistic cyclist balancing response. The novel simulator's kinematics are representative of a bicycle's during road use, and surpass all existing lateral motion solutions. With this result, we have demonstrated that for realistic balancing behaviour, adding lateral motion related to a steering input is sufficient.

All participants were successful in using and balancing the simulator within a brief accustomisation period. Velocity-normalised system gains relating a steer input to bicycle sway and yaw motions, recorded on the simulator, did not differ substantially from those recorded outdoors. In terms of phase, the relation between steer, yaw and sway on the simulator is degraded with respect to outdoor cycling, due to delays introduced by the simulator and drive algorithm. However, participants have shown themselves to be adaptive to these delays, and they proved to be no real challenge for them. Steer-to-roll behaviour showed similar results, although gains differed more between simulator and outdoor cycling.

Subjectively speaking, the simulator and outdoor cycling elicit a similar cycling experience from its users, but care needs to be taken in interpreting the subjective scores in this study. As such, further subjective evaluation is a goal for future research.

Note

1. External 55" monitor, 4K resolution monitor (outline 1.228 × 0.702 m, width by height).

Disclosure statement

No potential conflict of interest was reported by the author(s).

References

[1] Saris. Mp1 Nfinity trainer platform; 2021 [cited 2021 Oct 23]. Available from: https://www.saris.com/product/mp1.
[2] LifeLine. Lifeline rocker plaat; 2021 [cited 2021 Oct 23]. Available from: https://www.wiggle.nl/lifeline-rocker-plaat.
[3] Zwift. Smart trainers; 2020. Available from: https://zwift.com/eu.
[4] Hernández-Melgarejo G, Flores-Hernández D, Luviano-Juárez A, et al. Mechatronic design and implementation of a bicycle virtual reality system. ISA Trans. 2019;97:336–351. doi: 10.1016/j.isatra.2019.08.002
[5] Schramka F, Arisona S, Joos M, et al. Development of virtual reality cycling simulator. JCP. 2018;13(6):603–605. doi: 10.17706/jcp.13.6.603-615
[6] Dialynas G, Schwab A, Happee R. Design and hardware selection for a bicycle simulator. Mech Sci. 2019;10:1–10. doi: 10.5194/ms-10-1-2019
[7] Tang Y, Tsoi M, Fong D, et al. The design of a virtual cycling simulator. Lect Notes Comput Sci. 2007;4469:162–170. doi: 10.1007/978-3-540-73011-8

[8] O'Hern S, Oxley J, Stevenson M. Validation of a bicycle simulator for road safety research. Accid Anal Prev. 2017;100:53–58. doi: 10.1016/j.aap.2017.01.002
[9] Shoman MM, Imine H. Bicycle simulator improvement and validation. IEEE Access. 2021;9:55063–55076. doi: 10.1109/ACCESS.2021.3071214
[10] Powell J. Hardware design for an electro-mechanical bicycle simulator in an immersive virtual reality environment [master's thesis]. University of Iowa; 2017.
[11] Kikuchi T. Development of virtual reality bike with cylindrical MR fluid brake. In: Proceedings of the 2012 IEEE International Conference on Robotics and Biomimetics, December 11–14, 2012, Guangzhou, China; 2012. p. unknown.
[12] Yap H, Tan C, Taha Z, et al. Design and development of a spatial immersive track cycling simulator. J Mov Health Exerc. 2018;2(7):39–52.
[13] He Q, Fan X, Ma D. Full bicycle dynamic model for interactive bicycle simulator. J Comput Inf Sci Eng. 2005;5(4):373–380. doi: 10.1115/1.2121749
[14] Schulzyk O, Bongartz J, Bildhauer T, et al. A bicycle simulator based on a motion platform in a virtual reality environment. Advances in Medical Engineering Springer Proceedings in Physics, vol 114 Springer, Berlin, Heidelberg. 2007.
[15] Kwon D, Yang G, Lee C, et al. Kaist interactive bicycle simulator. Proc – IEEE Int Conf Robot Autom. 2001;3:2313–2318.
[16] Wintersberger P, Matviienko A, Schweidler A, et al. Development and evaluation of a motion-based VR bicycle simulator. Proc ACM Hum-Comput Interact. 2022 sep;6(MHCI):1–19. doi: 10.1145/3546745
[17] Westerhof BE, de Vries EJH, Happee R, et al. Evaluation of a Motorcycle Simulator. Proceedings, Bicycle and Motorcycle Dynamics 2019, Symposium on the Dynamics and Control of Single Track Vehicles, 9–11 September 2019, University of Padova, Italy. 2020; https://bmd2019.figshare.com/articles/conference_contribution/Evaluation_of_a_Motorcycle_Simulator/11744328.
[18] Schwab A, Meijaard J. A review on bicycle dynamics and rider control. Veh Syst Dyn: Int J Veh Mech Mobility. 2013;51(7):1059–1090. doi: 10.1080/00423114.2013.793365
[19] Goetz T, von Drais von Sauerbronn K. Draisinen. J Für Literatur, Kunst, Luxus Und Mode. 1820;35:365–377.
[20] Rankine W. On the dynamical principles of the motion of velocipedes. Engineer. 1869, 1870;28, 29:79, 129, 153, 175, 2.
[21] Kooijman J, Schwab A, Moore J. Some observations on human control of a bicycle. In: Proceedings of the ASME 2009 Internation Design Engineering Technical Conferences and Computers and Information in Engineering Conference, IDETC/CIE 2009 (August 30–September 2, San Diego, CA). American Society of Mechanical Engineers, New York; 2009. p. 8. Paper No. DETC2009-86959.
[22] Moore J, Kooijman J, Schwab A, et al. Rider motion identification during normal bicycling by means of principal component analysis. Multibocy Syst Dyn. 2011;2(25):3–4.
[23] Kooijman J, Meijaard J, Papadopoulos J, et al. A bicycle can be self-stable without gyroscopic or caster effects. Sci Mag. 2011;332(6027):339–342.
[24] Meijaard J, Papadopoulos J, Ruina A, et al. Linearized dynamics equations for the balance and steer of a bicycle: a benchmark and review. Proc R Soc A. 2007;463:1955–1982. doi: 10.1098/rspa.2007.1857
[25] Parker. Ospe32-bhd belt driven, square rail bearing, rodless linear actuator; 2021. [cited 2021 Aug 30]. Available from: https://ph.parker.com/us/en/ospe32-bhd-belt-driven-square-rail-bearing-rodless-linear-actuator.
[26] Tacx. Tacx desktop app; 2021. [cited 2021 Aug 24]. Available from: https://www.microsoft.com/nl-nl/p/tacx-desktop-app/9nln5vxq40kx?activetab=pivot:overviewtab.
[27] Grottoli M, Mulder M, Happee R. Motorcycle simulator subjective and objective validation for low speed maneuvering. Proc Inst Mech Eng, Part D: J Automobile Eng. 2023;237(9):2175–2189. doi: 10.1177/09544070221110930
[28] Cain S, Ashton-Miller J, Perkins N. On the skill of balancing while riding a bicycle. PLoS ONE. 2016;11(2):e0149340. doi: 10.1371/journal.pone.0149340

[29] Moore J. Human control of a bicycle [dissertation]. University of California; 2012.
[30] Cain S. An experimental investigation of human/bicycle dynamics and rider skill in children and adults [dissertation]. Ann Arbor (MI): University of Michigan. 2013.
[31] Cain S. Measurement of bicycle and rider kinematics during real-world cycling using a wireless array of inertial sensors. In: Proceedings, Bicycle and Motorcycle Dynamics 2016, Symposium on the Dynamics and Control of Single Track Vehicles, 21–23 September 2016, Milwaukee, Wisconsin USA; 2016. p. unknown.
[32] Wang P, Yi J. Dynamic stability of a rider-bicycle system: Analysis and experiments. In: 2015 American Control Conference, Palmer House Hilton, July 1–3, 2015. Chicago, IL, USA; 2015. p. unknown.
[33] Dozza M, Fernandez A. Understanding bicycle dynamics and cyclist behaviour from naturalistic field data. IEEE Trans Intell Transp Syst. 2014;15(1):376–384. doi: 10.1109/TITS.2013.2279687
[34] Sanjurjo E, Naye M, Cuadrado J, et al. Roll angle estimator based on angular rate measurements for bicycles. Veh Syst Dyn. 2019;57(11):1705–1719. doi: 10.1080/00423114.2018.1551554
[35] Kovácsová N, de Winter J, Schwab A, et al. Riding performance on a conventional bicycle and a pedelec in low speed exercises: objective and subjective evaluation of middle-aged and older persons. Transp Res Part F. 2016;42:28–43. doi: 10.1016/j.trf.2016.06.018
[36] Ljung L. System identification-theory for the user. 2nd ed. Upper Saddle River, NJ: PTR Prentice-Hall; 1999.
[37] Kennedy R, Lane N, Berbaum K, et al. Simulator sickness questionnaire: an enhanced method for quantifying simulator sickness. Int J Aviat Psychol. 1993;3(3):203–220. doi: 10.1207/s15327108ijap0303_3
[38] Grottoli M. Development and evaluation of a motorcycle riding simulator for low speed maneuvering [dissertation]. Delft University of Technology; 2020.
[39] Groen E, Bos J. Simulator sickness depends on frequency of the simulator motion mismatch: an observation. Presence. 2008;17(6):584–593. doi: 10.1162/pres.17.6.584
[40] Wilson M, Beadle S, Kinsella A, et al. Task performance in a head-mounted display: the impacts of varying latency. Displays. 2020;61:101930. doi: 10.1016/j.displa.2019.101930
[41] Matsangas P, McCauley M, Becker W. The effect of mild motion sickness and sopite syndrome on multitasking cognitive performance. Hum Factors. 2014;56(6):1124–1135. doi: 10.1177/0018720814522484
[42] Bos J. Less sickness with more motion and/or mental distraction. J Vestib Res. 2015;25(1):23–33. doi: 10.3233/VES-150541
[43] Bruni S, Meijaard J, Rill G, et al. State-of-the-art and challenges of railway and road vehicle dynamics with multibody dynamics approaches. Multibody Syst Dyn. 2020;49(1):1–32. doi: 10.1007/s11044-020-09735-z
[44] Mittelstaedt J, Wacker J, Stelling D. Effects of display type and motion control on cybersickness in a virtual bike simulator. Displays. 2018;51:43–50. doi: 10.1016/j.displa.2018.01.002
[45] Reason J, Brand J. Motion sickness. London: Academic Press; 1975.
[46] Jamson H. Driving simulation validity: issues of field of view and resolution. In Proceedings of the driving simulation conference; 2000 Sep 6; p. 57–64.